Published in final edited form as:
Cell. 2013 August 1; 154(3): . doi:10.1016/j.cell.2013.07.005.

AMPD2 Regulates GTP Synthesis and is Mutated in a Potentially-Treatable Neurodegenerative Brainstem Disorder

Naiara Akizu[1,#], **Vincent Cantagrel**[1,15,#], **Jana Schroth**[1], **Na Cai**[1], **Keith Vaux**[1], **Douglas McCloskey**[2], **Robert K. Naviaux**[3], **Jeremy Van Vleet**[4], **Ali G. Fenstermaker**[1], **Jennifer L. Silhavy**[1], **Judith S. Scheliga**[5], **Keiko Toyama**[6], **Hiroko Morisaki**[6], **Fatma Mujgan Sonmez**[7], **Figen Celep**[8], **Azza Oraby**[9], **Maha S. Zaki**[10], **Raidah Al-Baradie**[11], **Eissa Faqeih**[12], **Mohammad Saleh**[12], **Emily Spencer**[1], **Rasim Ozgur Rosti**[1], **Eric Scott**[1], **Elizabeth Nickerson**[13], **Stacey Gabriel**[13], **Takayuki Morisaki**[6], **Edward W. Holmes**[14], and **Joseph G. Gleeson**[1,*]

[1]Neurogenetics Laboratory, Institute for Genomic Medicine, Rady Children's Hospital, Howard Hughes Medical Institute, University of California, San Diego, CA 92093, USA

[2]Department of Bioengineering, University of California, San Diego, CA 92093, USA

[3]Division of Biochemical Genetics and Metabolism, University of California, San Diego, CA 92093, USA

[4]Glycotechnology Core Resource, University of California, San Diego, CA 92093, USA

[5]Signal Transduction Program, Sanford-Burnham Medical Research Institute, La Jolla, CA 92037, USA

[6]Department of Bioscience and Genetics, National Cerebral and Cardiovascular Center Research Institute and Department of Molecular Pathophysiology, Osaka University Graduate School of Pharmaceutical Sciences, Osaka, 565-8565 Japan

[7]Department of Pediatric Neurology, Turgut Ozal University, Ankara, Turkey

[8]Medical Biology Department, Karadeniz Technical University, Trabzon, 61080, Turkey

[9]Pediatric Neurology Department, Cairo University Children's Hospital, Cairo 406, Egypt

[10]Clinical Genetics Department, Human Genetics and Genome Research Division, National Research Centre, Cairo 12311, Egypt

[11]Division of Pediatric Neurology, King Fahd University Hospital, Dammam, 31444, Kingdom of Saudi Arabia

[12]Division of Medical Genetics, Department of Pediatrics, King Fahad Medical City, Children's Hospital, Riyadh 11525, Kingdom of Saudi Arabia

[13]The Broad Institute of MIT and Harvard, Cambridge, MA 02141, USA

[14]Sanford Consortium for Regenerative Medicine, La Jolla, CA 92037, USA

[*]Correspondance: jogleeson@ucsd.edu (J.G.G.).
[15]Present address: INSERM U781, Institut IMAGINE, Hôpital Necker-Enfants Malades, 75015 Paris, France.
[#]These authors contributed equally to this work

Abstract

Purine biosynthesis and metabolism, conserved in all living organisms, is essential for cellular energy homeostasis and nucleic acids synthesis. The *de novo* synthesis of purine precursors is under tight negative feedback regulation mediated by adenosine and guanine nucleotides. We describe a new distinct early-onset neurodegenerative condition resulting from mutations in the *adenosine monophosphate deaminase 2* gene (*AMPD2*). Patients have characteristic brain imaging features of pontocerebellar hypoplasia (PCH), due to loss of brainstem and cerebellar parenchyma. We found that AMPD2 plays an evolutionary conserved role in the maintenance of cellular guanine nucleotide pools by regulating the feedback inhibition of adenosine derivatives on *de novo* purine synthesis. *AMPD2* deficiency results in defective GTP-dependent initiation of protein translation, which can be rescued by administration of purine precursors. These data suggest *AMPD2*-related PCH as a new, potentially treatable early-onset neurodegenerative disease.

Keywords

Purine; pyrimidine; deaminase; salvage; translation; GTP; *de novo* synthesis; neurodegeneration

INTRODUCTION

Neurodegenerative diseases including Parkinson's, Alzheimer's and Huntington's disease are defined by their progressive loss of structure or function of anatomically defined groups of neurons. Neurodegenerative diseases affecting children are at the most severe end of the spectrum, often affecting key regulatory enzymes in neuronal function and energy metabolism. These diseases include lysosomal, peroxisomal and mitochondrial defects such as Tay-Sach, Zellwegger and Leigh syndrome, respectively, resulting in a host of specific early-onset neurodegenerative phenotypes. While significant progress has been made in the underlying pathogenesis for both the adult and pediatric forms of disease, treatment currently remains out of reach for most patients (Thompson and Levitt, 2010).

Much of cerebellar growth occurs after birth (Rakic and Sidman, 1970), and therefore early onset degeneration is impossible to differentiate from hypoplasia. Pontocerebellar hypoplasia (PCH) represents a group of rare inherited progressive neurodegenerative disorders with prenatal onset and up to seven subtypes, with clear evidence for time-dependent loss of brain parenchyma (Barth, 1993; Maricich et al., 2011; Namavar et al., 2011). The defect is observed at birth, and thus the condition was initially considered as a hypoplasia, but degenerative features are fully documented (Namavar et al., 2011). Additional features of PCH include progressive microcephaly, defects of the corpus callosum, and clinical features of swallowing and feeding difficulties along with limb spasticity. Death usually results from chronic medical complications within the first 10 years of life, and no treatments exist.

Mutations in the evolutionarily conserved tRNA splicing endonuclease (TSEN) complex including *TSEN54, TSEN34*, and *TSEN2* were identified in some PCH patients to date (Budde et al., 2008), presumably implicating a protein synthetic defect in the disorder. In addition, PCH is associated with mutations in the *CHMP1A* gene, a regulator of BMI1-INK4A (Mochida et al., 2012) and in the RNA exosome component gene *EXOSC3* in a subvariant of PCH involving spinal motor neuron degeneration (Wan et al., 2012). Thus a host of pathways regulating RNA biology, polycomb signaling and protein synthesis interplay in the etiology of PCH.

Purine nucleotide metabolism is one of the most studied processes in biology, critical for synthesis of ATP and GTP to meet requirements both for energy production and nucleic acid

synthesis (Nyhan, 2005). The *de novo* purine synthetic pathway initiates with ribose-5-phosphate conversion to inosine monophosphate (IMP), which is then converted to either ATP or GTP, depending upon cellular requirements. The salvage pathway converts hypoxanthine and guanine to IMP and GMP respectively, through the enzyme hypoxanthine-guanine phosphoribosyltransferase (HGPRT), which is mutated in Lesch-Nyhan syndrome. Adenine salvage to AMP occurs through adenine phosphoribosyltransferase, mutated in some patients with renal failure. Although these fundamental steps are understood at the biochemical level, the mechanisms of cellular vulnerability to purine toxicity are not well understood, and other than in Lesch-Nyhan syndrome, neurological consequences are rarely described (Camici et al., 2010).

In this study, we identify AMPD2 as necessary for guanine nucleotide biosynthesis and protein translation. Our data provide evidence that AMP deaminase activity is critical during neurogenesis. We describe a new syndrome of PCH in five families caused by a defect in this enzymatic step that can be overcome at the cellular level by administration of a purine nucleotide precursor.

RESULTS

Identification of *AMPD2* mutations in a new pontocerebellar hypoplasia-like syndrome

In order to identify new causes of pontocerebellar hypoplasia, we recruited a cohort of 30 probands and their families with a presumptive diagnosis of PCH. We previously excluded cases with overlapping conditions such as Walker-Warburg syndrome, cortical pachygyria or evidence of altered metabolism such as elevations of serum lactate or abnormal peaks on standard clinical serum tandem mass spectroscopy. From these 30 families, 23 had documented parental consanguinity (first or second cousin marriages) and 21 displayed more than one affected member, consistent with the recessive mode of inheritance for PCH. Of the 30 probands, most had evidence of mild to moderate microcephaly, hypotonia/spasticity of the limbs, and progressive contractures. All patients had the classical MRI features of PCH (cerebellum and pontine size reduced at least by 50%), and were enrolled in this IRB-approved genetic study.

Exome sequence was generated in 68 individuals, from either two probands (from multiplex families) or both parents and affected (from simplex families) and interrogated for homozygous, compound heterozygous and *de novo* sequence changes and compared with our in-house database from 1500 Middle Eastern exomes. One family each had a demonstrable mutation in *EXOSC3* and *TSEN2*, and three families had mutations in *TSEN54*, all of which were predicted to be damaging to protein function and which segregated according to a strictly recessive mode of inheritance. The results validated our recruitment strategy for PCH, and suggested potentially new causes in the remaining families. While several potentially mutated genes emerged from this screen, one was recurrent, the *adenosine monophosphate deaminase-2* gene (*AMPD2*).

AMPD2 encodes one of three known AMP deaminase homologues, which converts AMP to IMP. In total, five unique homozygous mutations in *AMPD2* were independently identified in this cohort (Figure 1A–B), including two predicted premature stop codons: one in family PCH-1022 and the other one within the most significant linkage interval in family PCH-1298 (Figure S1A). The other three mutations occur in alpha helixes and alter the charge, polarity or helical propensity of highly conserved amino acids (Figure 1C, S1B) (Pace and Scholtz, 1998), predicted to disrupt key hydrogen bonds involved in protein integrity (Figure S1B) modeled on the solved structure of Arabidopsis AMP deaminase (Han et al., 2006). Sanger sequencing confirmed that all five mutations segregated according to a strictly recessive model of inheritance with full penetrance (Figure S1C). These variants

were not present in our in house exome sequences of additional 1500 individuals or in publically available SNP databases. The results suggest that *AMPD2* loss results in PCH.

Comparing brain MRI features among the five patients, we retrospectively identified a pathognomonic structural brain anomaly distinct from other patients with PCH, which we propose as PCH type 9. In all patients, there was hypoplasia/atrophy of the cerebellum, with a fluid-filled posterior fossa (mega cisterna magna) and flattening of the ventral part of the pons. The unique finding was present on axial images, in which the brainstem takes on a "Figure 8" appearance, with relative preservation of the cerebellar vermis. There was also generalized atrophy of the cerebral cortex and severe corpus callosum hypoplasia. (Figures 1A, S1D, and Table S1), but other organs were spared.

AMPD2 is a functional ortholog of yeast *AMD1* gene

AMPD2 is one of three paralogs in mammals mediating the conversion of AMP to IMP (Bausch-Jurken et al., 1992), all branched from a single ancestral *AMP Deaminase* gene common with *AMD1* (Figure 2A), the unique AMP deaminase in *Saccharomyces cerevisiae* (Meyer et al., 1989). Human AMPD2 has the most sequence similarity to AMD1 (53% identity and 69% similarity over 623 amino acids), as compared with AMPD1 and 3. Individuals with *AMPD1* homozygous mutations display Myoadenylate deaminase deficiency (MIM+102770), possibly the most prevalent genetic disease in humans. However, only a small percent of homozygous-deficient individuals show symptoms, including exercise-stress-induced accumulation of AMP with resultant muscle weakness and cramping (Fishbein et al., 1978). *AMPD3* shows homozygous inactivating mutations in healthy individuals (Ogasawara et al., 1987), with increased adenosine nucleotide levels in erythrocytes (MIM#612874). RT-PCR analysis of the gene family in human tissue shows expression of *AMPD1* predominantly restricted to muscle but *AMPD2* and -*3* with widespread expression (Figure S2A).

To determine whether human *AMPD2* is a functional ortholog of yeast *AMD1*, we expressed *AMPD2* in the yeast *amd1* mutant (Jones, 1982). As previously reported (Saint-Marc et al., 2009), this mutant shows a strong germination and/or growth of spores phenotype in the presence of adenine, which is rescued by forced expression of yeast *AMD1* under the tetracycline response element (Figure S2B). Presumably, the presence of exogenous adenine effectively stresses the cells, resulting in further accumulation of adenosine nucleotides. Using the same vector system, we found that human *AMPD2* cDNA showed near complete rescue of growth (Fig. 2B).

AMPD2 mutations are deleterious for protein function

We next expressed in the yeast *amd1* mutant each of the identified patient mutations introduced in the *AMD1* gene, in order to test for altered activity. In the presence of doxycycline, *AMD1* rescued the *amd1* phenotype but mutated versions of the yeast gene failed to complement the growth defect (Figure 2C). We conclude that the patient mutations represent null alleles. Some residual activity was however observed in conditions of over-expression for mutations E721D and R674H (Figure S2C) suggesting some patient missense mutations may maintain minimal residual activity.

In order to determine the effect of mutations on protein function in mammalian cells at physiological expression levels, we obtained skin fibroblast cultures from patients and one unaffected parent in three different families. AMPD2 protein was nearly completely absent in patient cells (Figure 2D). By the assessment of AMP deaminase activity from lysed patient cells in the presence of exogenous AMP (Kirkwood et al., 2012), we found reduction of 80–90% of activity (Figure 2E), suggesting no compensatory effect by AMPD3

expression in these cells (Figure S2D). We conclude that patient cells show severe reductions in AMPD2 levels and AMP deaminase activity.

Survival is compromised in challenged *AMPD2* mutant cells

The near complete absence of enzymatic AMP deaminase activity prompted a search for a phenotype in patient cells. However, we found cell growth and survival of fibroblasts were unaffected under basal growth conditions, and no evidence of altered purine nucleotide levels (Figure S3A–B). The *amd1* yeast mutant shows growth restriction only in the presence of exogenous adenine, which feeds directly into AMP through APRT (Alfonzo et al., 1997), thus we considered that addition of exogenous purines to these cells might uncover relevant phenotypes. We utilized adenosine, which is both bioavailable and feeds into AMP through Adenosine kinase (Figure 3A), and found a dose-dependent effect on cell survival in patient fibroblasts in the range of 50–500μM concentrations, dropping to about half of untreated survival rates. Cells from unaffected family members showed no effect of adenosine at these concentrations (Figure 3B–C). We conclude that, like the yeast *amd1* mutant, metabolic stress is required to uncover phenotypic consequences in *AMPD2* mutant cells.

To study the mechanism of human neuronal vulnerability in *AMPD2* mutants, we generated induced pluripotent stem cells (iPSCs) from families PCH-1298 and PCH-1236, from both affecteds (*AMPD2* homozygous mutants) and unaffecteds (heterozygous controls). Because there is generalized brain affection in PCH9 patients (including microcephaly and corpus callosum involvement), we reasoned that standard neural induction protocol derived cells might capture the neuronal vulnerability observed in patients. We demonstrated pluripotency, differentiation to three germ layers after embryoid body formation and generation of neural progenitor cells (NPCs) using standard methods of derivation (Chambers et al., 2009) (Figure 3D and S3C). Growth rates and purine nucleotide levels were indistinguishable in standard culture medium (Figure S3D–E), as were survival of neural progenitor cells. We confirmed the absence of AMPD2, and a nearly complete lost of AMP deaminase activity (Figure S3F).

Standard NPC medium lacks adenosine (Table S2), whereas concentrations from 20nM to 300μM are well documented in mammalian brain (Rathbone et al., 1999). Thus we tested a range of adenosine concentrations and found that the survival of *AMPD2* mutant but not control NPCs dropped considerably at concentration as low as 5μM (Figure 3E–F), which is an order of magnitude more sensitive than the isogenic patient fibroblasts. To test for specificity of the effect, we transduced affected NPCs with either *AMPD2* or a fluorescent tag and found restoration of survival specifically following AMPD2 transduction (Figure S3G). Thus, the addition of physiological adenosine concentrations to the *AMPD2* mutant cells can recapitulate the neural specific defect observed in patients, providing a model to further explore the underlying mechanisms leading to neurodegeneration.

Altered adenosine and guanine nucleotides in *AMPD2* mutant cells

We predicted that cellular uptake of adenosine is necessary for cellular toxicity in *AMPD2* mutant cells. We thus treated NPCs with 5-Iodotubercidin to inhibit adenosine uptake, and found it efficiently blocked adenosine toxicity (Figure S4A). In contrast, treatment with the adenosine receptor antagonist CSG15943 did not rescue adenosine-mediated toxicity, and the class P1 purinergic receptor agonist NECA was not sufficient to compromise survival (Figure S4A–B). We conclude that intracellular accumulation of adenosine and derived nucleotides and not activation of purinergic signaling through cognate receptors underlie the neurotoxicity.

Because AMPD2 executes AMP deamination, inactivating mutations predict an accumulation of adenosine nucleotides. We measured nucleotide levels in patient fibroblasts treated with 50μM adenosine (the lowest toxic dose), and found elevated ATP levels, more striking in *AMPD2* homozygous mutant cells compared with heterozygous control cells (Figure 4A). As expected by the inability to deaminate AMP to IMP, there was also corresponding decrease in guanine nucleotides, which was again more striking in homozygous mutant cells (Figure 4B). The results were similar in NPCs cultured with 10μM adenosine for 5h (a time before compromised viability, Figure S4C). Patient NPCs showed a slight increase in adenosine nucleotides, most notably for ATP (Figure 4C), and a dramatic reduction in guanine nucleotides, most remarkable for GTP, which was reduced by half (Figure 4D). These demonstrate that patient cells show adenosine-dependent accumulation of specific adenosine nucleotides and depletion of guanine nucleotides.

De novo purine biosynthesis is inhibited in *AMPD2* mutant NPCs

The previous results led us to question why guanine nucleotide levels were reduced only in the presence of exogenous adenosine. In order to assess metabolic profiles more completely, we developed a quantitative mass spectroscopy panel of 140 metabolites (Table S3), and tested in unaffected and affected NPCs untreated and treated with two different adenosine concentrations. Adenosine itself, despite addition to the culture media, remained below detectable level, suggesting efficient cellular processing. Many of the analyzed metabolites responded to adenosine treatment similarly in unaffected and affected cells, probably reflecting shared metabolism. However, in accordance with HPLC data, adenosine nucleotide pools were increased slightly, and guanine nucleotide pools were notably decreased in homozygous mutant NPCs (Figure 4E, S4D, Table S4).

Purine nucleotides can exert inhibitory feedback on the *de novo* pathway by inhibiting PRPP synthetase and PRPP amidotransferase (Watts, 1983). We thus considered whether the accumulated adenosine nucleotides might additionally inhibit *de novo* purine biosynthesis, which could explain why adenosine treatment reduces guanine nucleotide levels. Several lines of evidence support this model. First, IMP was one of the most reduced compounds in affected NPCs compared with unaffected, suggesting a failure of *de novo* synthesis pathway to generate IMP. Second, IMP should theoretically be salvaged from hypoxanthine and PRPP by the HGPRT enzyme (Figure 3A). Despite the presence of hypoxanthine in the culture media, IMP was not replenished and cell growth was restricted, suggesting PRPP, which is synthesized by PRPP synthetase in the first step of the *de novo* pathway, is in limiting amounts. Third, 5-Aminoimidazole-4-carboxamide riboside (AICAr, i.e. dephosphorylated AICAR), an intermediate of *de novo* synthesis, was more severely reduced in affected than in unaffected NPCs treated with adenosine (Figure S4E). Finally, genome-wide expression profiles were compared with and without treatment. Despite few notable alterations, suggesting mostly acute biochemical and/or post-transcriptional derangements, there was an increase in *IMPDH2* levels (Figure S5A–C), which is known to increase upon guanine nucleotide depletion to support conversion of IMP to GMP (Escobar-Henriques and Daignan-Fornier, 2001).

Whereas the activity of *de novo* purine biosynthesis enzymes is high in proliferating cells such as NPCs, it is much lower in post-mitotic cells in general and in adult mammalian brain in particular (Watts, 1983). We predicted that if feedback inhibition contributes to the phenotype in proliferating NPCs, postmitotic neurons might be impervious to adenosine treatment. Both control- and patient-derived NPCs were induced towards neuronal differentiation, and acquired indistinguishable axon- and dendrite-like structures (Figure S4F). Exposure to adenosine in the medium had just a slight effect on survival that was not distinguishable from the effect in control cells at either 15- or 30-day timepoints (Figure

S4G). Together the data suggest that blockage of *de novo* purine nucleotides contributes to the cellular toxicity and guanine nucleotide depletion observed in patient cells.

AMP deaminase deficiency associates with altered nucleotide levels and degeneration in brain

In order to determine if these alterations in nucleotide levels are apparent in intact brain, we studied *Ampd2* and *Ampd3* knockout (KO) mice (Cheng et al., 2012; Toyama et al., 2012). The absence of histological phenotype in *Ampd2* KO brain (Figure 5A) and the co-expression of *Ampd2* and *Ampd3* in embryonic and postnatal mouse brains, both contributing equally to brain AMP deaminase activity (Figure 5B–C), prompted us to test for functional redundancy by generating *Ampd2* and *Ampd3* double knockout mice (DKO), which were born in the expected Mendelian ratio. Early after birth, DKOs were distinguishable from wild-type littermates by slightly reduced body weight and severely shortened lifespan limited to 2 or 3 weeks (Figure 5D). Besides the slightly reduced brain size, consistent with the body size reduction, *Ampd2/3* DKO mice brains showed little evidence of the characteristic neuronal loss observed in *AMPD2* mutant patients. After P14, we observed a neurodegenerative phenotype mostly affecting the CA3 pyramidal neurons in the hippocampus and some sparse pyknotic cells all over the cortex and the cerebellum (Figure 5E), associated with behavioral gait disturbance (Movie S1). Investigation of nucleotide levels in these brains at 2 weeks demonstrated 25% increase in ATP nucleotide levels and 33% decrease in GTP levels in DKO compared to WT (Figure 5F). These results indicate partial genetic redundancy for *Ampd2* and *Ampd3* in mouse brain and support a conserved role for AMP deaminase activity in neuroprotection through adenosine nucleotide metabolism and/or maintenance of the guanine nucleotide pool.

AICAr treatment rescues adenosine mediated toxicity in mutant cells

The previous data suggests accumulation of adenosine- and depletion of guanine-nucleotides, but did not distinguish relative importance in neurotoxicity. We reasoned that exogenous application of AICAr should allow us to distinguish these, as this would bypass a block in *de novo* synthesis towards guanine nucleotides, but only further exacerbate accumulation of adenosine nucleotides through the conversion of IMP to AMP. AICAr is bioavailable to cultured cells and converted to AICAR through adenosine kinase (Figure 6A). The growth phenotype of *amd1* yeast was almost completely rescued with increasing AICAr concentrations (Figure 6B), suggesting impaired *de novo* synthesis as a major defect.

We next examined if patient NPCs might respond similarly to AICAr treatments. However, because AICAr can compete with adenosine for internalization mediated by nucleoside transporters (Gadalla et al., 2004), we designed a timed protocol (Figure 6C). First we treated patient derived NPCs with adenosine for 7h, followed by wash-out and culture with standard media for an additional 17h. With this protocol, survival of *AMPD2* mutant NPCs was similar to cells under continued exposure to adenosine, suggesting lingering toxicity of adenosine. When the media was instead supplemented with AICAr, we noted concentration-dependent rescued viability (Figure 6D). Concurrently, following the AICAr protocol, guanine nucleotide levels were restored to near normal levels (Figure 6E), and genome-wide expression profile demonstrated partial restoration of *IMPDH2* level (Figure S5C), suggesting relief of cellular stress.

AMP protein kinase (AMPK) activation is a well-documented effect of AICAr, which was also observed in affected NPCs (Figure S5D). However, substituting AICAr with Metformin, an AMPK activator that does not directly feed into *de novo* purine synthesis, failed to rescue adenosine-mediated toxicity (Figure S5E), excluding AMPK activation as a rescue mechanism. This, together with confirmation by mass spectroscopy that IMP is

significantly restored by AICAr treatment (Figure 6F), supports the *de novo* purine synthesis as the major target for guanine nucleotide replenishment in AMPD2 mutant cells.

Translation initiation is blocked in AMP deaminase-deficient cells

Because the established PCH genes implicate defective protein synthesis, and because GTP is the main energy source in protein synthesis, we considered GTP depletion could impair protein synthesis in AMPD2 mutant PCH patients. Protein synthesis can be assessed at a global level using [35]S-methionine metabolic labeling, which showed a severe defect in patient derived NPCs following adenosine treatment (Figure 7A). This finding was confirmed in the *amd1* yeast strain, showing a decrease of about 40% incorporation in acid-insoluble material, a defect completely rescued in a time-dependent fashion with the addition of AICAr in the culture media (Figure 7B).

In order to understand this mechanism, we analyzed polyribosome profiles from *amd1* and WT strains and found a decrease in relative amount of actively translating ribosomes (considered as the polyribosome) in the *amd1* mutant (Figure 7C). The decreasing ratio of polyribosome over monosome (80S peak) in the mutant cells (respectively 2.9 and 1.7 for WT and *amd1* strains) suggested a defect in protein translation initiation, as has been documented for eIF2 (eukaryotic translation initiation factor 2) GTP-dependent activation (Foiani et al., 1991) or guanine nucleotide depleted cells caused by GMP synthase mutation (Iglesias-Gato et al., 2011). As a comparison, we evaluated a *SEN2* mutant, encoding a highly conserved member of the tRNA splicing endonuclease (SEN) complex in yeast, which is orthologous to the human *TSEN2* gene and mutated in PCH type 2 (MIM 608753). We found that the temperature-sensitive mutant *sen2–41*, which affects tRNA splicing (Yoshihisa et al., 2003), also showed a pronounced decrease in [35]S-methionine metabolic labeling at non permissive temperature (Figure 7D), suggesting protein translation defect as a common mechanism in PCH.

DISCUSSION

Neuronal vulnerability in *AMPD2* mutants

Adenosine toxicity is a well-recognized consequence of metabolic derangements and includes a number of downstream consequences such as pyrimidine/purine starvation and defects in methylation (Archer et al., 1985). Our study demonstrates that neural cells deficient in AMPD activity are exquisitely sensitive to adenosine, which is generated in neural tissue by physiological processes such as active methylation and synaptic activity (Rathbone et al., 1999). The vulnerability of *AMPD2* mutant neurons to physiological levels of adenosine, mediating cellular growth restriction followed by cell death, is likely a consequence of guanine nucleotide depletion.

Why do humans show specific vulnerabilities of brainstem structures to *AMPD2* mutations? This may reflect regional differences in expression of other AMPD homologs. Indeed, while *AMPD2* and *AMPD3* are co-expressed in developing human cerebral cortex, *AMPD2* is the major homolog in the cerebellum (Figure S2A). This, however, does not apply for mouse brain, where the two homologs, present in cortex and cerebellum, contribute equally to brain AMP deaminase activity. Accordingly, we only observe neuronal vulnerability, resulting in ataxia and cell loss, when both *Ampd2* and *Ampd3* are deleted in mice. This is reminiscent of HPRT deficiency, leading to Lesch-Nyhan syndrome in humans but to which mice show no consequence unless additional purine metabolism enzymes are pharmacologically inhibited (Wu and Melton, 1993). Thus, although the simplest interpretation is that vulnerability to *AMPD2* mutations is uncovered when *AMPD3* compensatory effect is lacking, there may be additional buffering of purine metabolism vulnerability in mice.

Protein translation impairment and neurodegeneration

Known mutations in a wide range of animal models and human disorders suggest misregulation of protein translation as a pathogenic mechanism of neurodegeneration. In the *sticky* mouse, neurodegeneration is caused by the mutation of an amino-acyl-tRNA synthetase, which disrupts translation fidelity and causes accumulation of misfolded proteins (Lee et al., 2006). Mutations in the protein synthesis factor *Eef1a2* causes neurodegeneration in the *Wasted* mouse, presumably due to a tissue-specific block of protein translation (Scheper et al., 2007). Similarly, in humans, the five *EIF2B* genes that encode translation initiation factors are each mutated in childhood ataxia with central nervous system hypomyelinization (CACH, MIM#603896). In PCH the most common mutations fall in three of the four known subunits of tRNA endonuclease complex (TSEN54, TSEN34 and TSEN2) (Budde et al., 2008), which presumably affect tRNA processing and downstream protein translation, but not yet demonstrated in patient cells. While we did not fully explore other global consequences of GTP depletion such as on RNA or DNA synthesis (Cohen et al., 1981), our identification of similar protein synthesis defects in AMP deaminase deficient cells and in yeast mutant for *sen2* (*TSEN2* ortholog) suggests that reduced protein synthesis may be a common pathogenic mechanism for neurodegeneration in PCH.

Enhancement of *de novo* purine biosynthesis as therapeutic target

We identified deficiency in guanine nucleotides as central to the *AMPD2* pathogenesis, and linked this to defective protein synthesis. There are other requirements for guanine nucleotides to meet cellular energy and signaling demands including G-protein signaling and microtubule polymerization, which we do not evaluate here. Deficiency of guanine nucleotides as central to the pathogenesis was supported by AICAr treatment, which rescue GTP depletion, protein synthesis error and cell survival phenotype. Might this serve as a potential treatment in patients? AICAr is proven to be beneficial for exercise endurance by means of AMPK activation, the master regulator of cellular energy metabolism (Narkar et al., 2008). However, by targeting the same pathway, AICAr can inhibit axon growth in mouse cultured cortical neurons (Williams et al., 2011). AICAr's effects on nucleotide metabolism are disparate, showing biphasic effects on cell survival what responses to an inhibitory effect on pyrimidine nucleotide biosynthesis at intermediate concentrations (Thomas et al., 1981). Therefore, if AICAr is to be used therapeutically, thorough evaluation of effective non-toxic dosage would be required. While AICAr's potential as therapeutic treatment remains to be studied, enhancing *de novo* purine biosynthesis might be efficient in the treatment of PCH type9.

METHODS

Patient recruitment

Patients were enrolled and sampled according to standard local practice in approved human subjects protocols at the University of California.

Exome sequencing

DNA was extracted from peripheral blood leukocytes by salt extraction. Exon capture, sequencing, variant calling and filtering were performed as previously described (Dixon-Salazar et al., 2012). For specific details see Extended Experimental Procedures.

Yeast strains and culture conditions

To generate the *S. cerevisiae amd1* mutant strain, the *AMD1/YML035C* ORF was replaced by PCR-based gene targeting with the hphNT1 marker (Janke et al., 2004) in the haploid

reference strain BY4741. Yeast cultures were grown as described (Saint-Marc et al., 2009). For specific details see Extended Experimental Procedures.

Fibroblasts culture, iPSC and NPC generation

Fibroblasts were generated from unaffected and affected dermal biopsies explants. iPSCs, neural progenitor cells and neurons were obtained as previously described (Chambers et al., 2009; Okita et al., 2011). For specific details see Extended Experimental Procedures.

Mouse

Animal use followed NIH guidelines and was approved by IACUC at the University of California San Diego. *Ampd2* (−/−) mice were previously generated (Toyama et al., 2012) and *Ampd3* (−/−) were either generated by us using ES cell clone EPD0043_3_B02 generated by the Wellcome Trust Sanger Institute (www.komp.org) or from previous publication (Cheng et al., 2012).

Growth curve and cell survival

Modified MTT method (Carmichael et al., 1987) was used for growth curve and survival analysis, detailed in Extended Experimental Procedures.

AMP deaminase activity assay

AMP deaminase activity was performed as previously described (Kirkwood et al., 2012) with minor modifications detailed in Extended Experimental Procedures.

Nucleotide analysis by HPLC

Nucleotide extraction was performed as previously described (Fairbanks et al., 2002) and nucleotides analyzed by HPLC. For specific details see Extended Experimental Procedures.

LC-MS/MS

Metabolites were extracted from with 80:20/0.1% Methanol:Water/Formic acid pre-cooled to −80C and ^{13}C-Labeled *E. coli* extract as an internal standard. Chromatographic separation was achieved using a UFLC XR HPLC (Shimadzu) and compounds were detected and quantified on an AB SCIEX Qtrap® 5500 mass spectrometer (AB SCIEX). For specific details see Extended Experimental Procedures.

Polysome profiling

Yeast extracts were prepared as described (Esposito et al., 2010). Typically 10 OD260 of nucleic acid were loaded onto an 11 ml linear sucrose gradient (10 to 50% w/v) and centrifuge using SW40Ti rotor (Beckman) at 39,000 rpm for 160 minutes at 4°C. Sample tubes were loaded on a tube piercer after priming the system with 55% sucrose and a flow rate of 800μl/min was set on the peristaltic pump. Absorbance at 254 was monitored using an Econo UV monitor (BioRad) and data were collected and analyzed with the WinDaq software (DATAQ Instruments).

Supplementary Material

Refer to Web version on PubMed Central for supplementary material.

Acknowledgments

We thank the families for their participation. We thank B. Daignan-Fornier and B. Pinson for the tet-AMD1 plasmid and helpful advices, A. Hopper and T. Yoshihisa for the sen2-41 yeast strain, E. Masliah and S. Michael

for human brain specimens, S.J. Elledge for pINDUCER20 plasmid. We thank T. Friedman, W. Nyhan, B. Barshop, R. Evans, J. Cheng and D. Wolf for helpful discussions. N.A. was supported by the California Institute for Regenerative Medicine. R.K.N. was supported by grants from the UCSD Christini Fund and the Jane Botsford Johnson Foundation. This work was supported by the NIH (P01HD070494, R01NS048453, and P30NS047101 for imaging support), Broad Institute grant U54HG003067 (to Eric Lander); the Center for Inherited Disease Research for genotyping; the Simons Foundation Autism Research Initiative. Exome data have been deposited into dbGaP (phs000288).

REFERENCES

Alfonzo JD, Sahota A, Taylor MW. Purification and characterization of adenine phosphoribosyltransferase from Saccharomyces cerevisiae. Biochim Biophys Acta. 1997; 1341:173–182. [PubMed: 9357956]

Archer S, Juranka PF, Ho JH, Chan VL. An analysis of multiple mechanisms of adenosine toxicity in baby hamster kidney cells. J Cell Physiol. 1985; 124:226–232. [PubMed: 3900094]

Barth PG. Pontocerebellar hypoplasias. An overview of a group of inherited neurodegenerative disorders with fetal onset. Brain Dev. 1993; 15:411–422. [PubMed: 8147499]

Bausch-Jurken MT, Mahnke-Zizelman DK, Morisaki T, Sabina RL. Molecular cloning of AMP deaminase isoform L. Sequence and bacterial expression of human AMPD2 cDNA. J Biol Chem. 1992; 267:22407–22413. [PubMed: 1429593]

Budde BS, Namavar Y, Barth PG, Poll-The BT, Nurnberg G, Becker C, van Ruissen F, Weterman MA, Fluiter K, te Beek ET, et al. tRNA splicing endonuclease mutations cause pontocerebellar hypoplasia. Nat Genet. 2008; 40:1113–1118. [PubMed: 18711368]

Camici M, Micheli V, Ipata PL, Tozzi MG. Pediatric neurological syndromes and inborn errors of purine metabolism. Neurochem Int. 2010; 56:367–378. [PubMed: 20005278]

Carmichael J, DeGraff WG, Gazdar AF, Minna JD, Mitchell JB. Evaluation of a tetrazolium-based semiautomated colorimetric assay: assessment of chemosensitivity testing. Cancer Res. 1987; 47:936–942. [PubMed: 3802100]

Chambers SM, Fasano CA, Papapetrou EP, Tomishima M, Sadelain M, Studer L. Highly efficient neural conversion of human ES and iPS cells by dual inhibition of SMAD signaling. Nat Biotechnol. 2009; 27:275–280. [PubMed: 19252484]

Cheng J, Morisaki H, Toyama K, Ikawa M, Okabe M, Morisaki T. AMPD3-deficient mice exhibit increased erythrocyte ATP levels but anemia not improved due to PK deficiency. Genes Cells. 2012; 17:913–922. [PubMed: 23078545]

Cohen MB, Maybaum J, Sadee W. Guanine nucleotide depletion and toxicity in mouse T lymphoma (S-49) cells. J Biol Chem. 1981; 256:8713–8717. [PubMed: 7263680]

Dixon-Salazar TJ, Silhavy JL, Udpa N, Schroth J, Bielas S, Schaffer AE, Olvera J, Bafna V, Zaki MS, Abdel-Salam GH, et al. Exome sequencing can improve diagnosis and alter patient management. Sci Transl Med. 2012; 4 138ra178.

Escobar-Henriques M, Daignan-Fornier B. Transcriptional regulation of the yeast gmp synthesis pathway by its end products. J Biol Chem. 2001; 276:1523–1530. [PubMed: 11035032]

Esposito AM, Mateyak M, He D, Lewis M, Sasikumar AN, Hutton J, Copeland PR, Kinzy TG. Eukaryotic polyribosome profile analysis. J Vis Exp. 2010

Fairbanks LD, Jacomelli G, Micheli V, Slade T, Simmonds HA. Severe pyridine nucleotide depletion in fibroblasts from Lesch-Nyhan patients. Biochem J. 2002; 366:265–272. [PubMed: 11996669]

Fishbein WN, Armbrustmacher VW, Griffin JL. Myoadenylate deaminase deficiency: a new disease of muscle. Science. 1978; 200:545–548. [PubMed: 644316]

Foiani M, Cigan AM, Paddon CJ, Harashima S, Hinnebusch AG. GCD2, a translational repressor of the GCN4 gene, has a general function in the initiation of protein synthesis in Saccharomyces cerevisiae. Mol Cell Biol. 1991; 11:3203–3216. [PubMed: 2038326]

Gadalla AE, Pearson T, Currie AJ, Dale N, Hawley SA, Sheehan M, Hirst W, Michel AD, Randall A, Hardie DG, et al. AICA riboside both activates AMP-activated protein kinase and competes with adenosine for the nucleoside transporter in the CA1 region of the rat hippocampus. J Neurochem. 2004; 88:1272–1282. [PubMed: 15009683]

Han BW, Bingman CA, Mahnke DK, Bannen RM, Bednarek SY, Sabina RL, Phillips GN Jr. Membrane association, mechanism of action, and structure of Arabidopsis embryonic factor 1 (FAC1). J Biol Chem. 2006; 281:14939–14947. [PubMed: 16543243]

Iglesias-Gato D, Martin-Marcos P, Santos MA, Hinnebusch AG, Tamame M. Guanine nucleotide pool imbalance impairs multiple steps of protein synthesis and disrupts GCN4 translational control in Saccharomyces cerevisiae. Genetics. 2011; 187:105–122. [PubMed: 20980241]

Janke C, Magiera MM, Rathfelder N, Taxis C, Reber S, Maekawa H, Moreno-Borchart A, Doenges G, Schwob E, Schiebel E, et al. A versatile toolbox for PCR-based tagging of yeast genes: new fluorescent proteins, more markers and promoter substitution cassettes. Yeast. 2004; 21:947–962. [PubMed: 15334558]

Jones, EWaFGR. Regulation of amino acid and nucleotide biosynthesis in yeast. In: Strathern, JNJ.; EW; Broach, JR., editors. In The Molecular Biology of the Yeast Saccharomyces: Metabolism and Gene Expression. Cold Spring Harbor, NY: Cold Spring Harbor Laboratory Press; 1982. p. 181-299.

Kirkwood JS, Lebold KM, Miranda CL, Wright CL, Miller GW, Tanguay RL, Barton CL, Traber MG, Stevens JF. Vitamin C deficiency activates the purine nucleotide cycle in zebrafish. J Biol Chem. 2012; 287:3833–3841. [PubMed: 22170049]

Lee JW, Beebe K, Nangle LA, Jang J, Longo-Guess CM, Cook SA, Davisson MT, Sundberg JP, Schimmel P, Ackerman SL. Editing-defective tRNA synthetase causes protein misfolding and neurodegeneration. Nature. 2006; 443:50–55. [PubMed: 16906134]

Maricich SM, Aqeeb KA, Moayedi Y, Mathes EL, Patel MS, Chitayat D, Lyon G, Leroy JG, Zoghbi HY. Pontocerebellar hypoplasia: review of classification and genetics, and exclusion of several genes known to be important for cerebellar development. J Child Neurol. 2011; 26:288–294. [PubMed: 21383226]

Meyer SL, Kvalnes-Krick KL, Schramm VL. Characterization of AMD, the AMP deaminase gene in yeast. Production of amd strain, cloning, nucleotide sequence, and properties of the protein. Biochemistry. 1989; 28:8734–8743. [PubMed: 2690949]

Mochida GH, Ganesh VS, de Michelena MI, Dias H, Atabay KD, Kathrein KL, Huang HT, Hill RS, Felie JM, Rakiec D, et al. CHMP1A encodes an essential regulator of BMI1-INK4A in cerebellar development. Nat Genet. 2012; 44:1260–1264. [PubMed: 23023333]

Namavar Y, Barth PG, Poll-The BT, Baas F. Classification, diagnosis and potential mechanisms in pontocerebellar hypoplasia. Orphanet J Rare Dis. 2011; 6:50. [PubMed: 21749694]

Narkar VA, Downes M, Yu RT, Embler E, Wang YX, Banayo E, Mihaylova MM, Nelson MC, Zou Y, Juguilon H, et al. AMPK and PPARdelta agonists are exercise mimetics. Cell. 2008; 134:405–415. [PubMed: 18674809]

Nyhan WL. Disorders of purine and pyrimidine metabolism. Mol Genet Metab. 2005; 86:25–33. [PubMed: 16176880]

Ogasawara N, Goto H, Yamada Y, Nishigaki I, Itoh T, Hasegawa I, Park KS. Deficiency of AMP deaminase in erythrocytes. Hum Genet. 1987; 75:15–18. [PubMed: 3804327]

Okita K, Matsumura Y, Sato Y, Okada A, Morizane A, Okamoto S, Hong H, Nakagawa M, Tanabe K, Tezuka K, et al. A more efficient method to generate integration-free human iPS cells. Nat Methods. 2011; 8:409–412. [PubMed: 21460823]

Pace CN, Scholtz JM. A helix propensity scale based on experimental studies of peptides and proteins. Biophys J. 1998; 75:422–427. [PubMed: 9649402]

Rakic P, Sidman RL. Histogenesis of cortical layers in human cerebellum, particularly the lamina dissecans. J Comp Neurol. 1970; 139:473–500. [PubMed: 4195699]

Rathbone MP, Middlemiss PJ, Gysbers JW, Andrew C, Herman MA, Reed JK, Ciccarelli R, Di Iorio P, Caciagli F. Trophic effects of purines in neurons and glial cells. Prog Neurobiol. 1999; 59:663–690. [PubMed: 10845757]

Saint-Marc C, Pinson B, Coulpier F, Jourdren L, Lisova O, Daignan-Fornier B. Phenotypic consequences of purine nucleotide imbalance in Saccharomyces cerevisiae. Genetics. 2009; 183:529–538. 521SI–527SI. [PubMed: 19635936]

Thomas CB, Meade JC, Holmes EW. Aminoimidazole carboxamide ribonucleoside toxicity: a model for study of pyrimidine starvation. J Cell Physiol. 1981; 107:335–344. [PubMed: 6166628]

Thompson BL, Levitt P. The clinical-basic interface in defining pathogenesis in disorders of neurodevelopmental origin. Neuron. 2010; 67:702–712. [PubMed: 20826303]

Toyama K, Morisaki H, Cheng J, Kawachi H, Shimizu F, Ikawa M, Okabe M, Morisaki T. Proteinuria in AMPD2-deficient mice. Genes Cells. 2012; 17:28–38. [PubMed: 22212473]

Wan J, Yourshaw M, Mamsa H, Rudnik-Schoneborn S, Menezes MP, Hong JE, Leong DW, Senderek J, Salman MS, Chitayat D, et al. Mutations in the RNA exosome component gene EXOSC3 cause pontocerebellar hypoplasia and spinal motor neuron degeneration. Nat Genet. 2012; 44:704–708. [PubMed: 22544365]

Watts RW. Some regulatory and integrative aspects of purine nucleotide biosynthesis and its control: an overview. Adv Enzyme Regul. 1983; 21:33–51. [PubMed: 6152730]

Williams T, Courchet J, Viollet B, Brenman JE, Polleux F. AMP-activated protein kinase (AMPK) activity is not required for neuronal development but regulates axogenesis during metabolic stress. Proc Natl Acad Sci U S A. 2011; 108:5849–5854. [PubMed: 21436046]

Wu CL, Melton DW. Production of a model for Lesch-Nyhan syndrome in hypoxanthine phosphoribosyltransferase-deficient mice. Nat Genet. 1993; 3:235–240. [PubMed: 8485579]

Yoshihisa T, Yunoki-Esaki K, Ohshima C, Tanaka N, Endo T. Possibility of cytoplasmic pre-tRNA splicing: the yeast tRNA splicing endonuclease mainly localizes on the mitochondria. Mol Biol Cell. 2003; 14:3266–3279. [PubMed: 12925762]

Research Highlights

- Mutations in *AMPD2*, an essential gene for purine metabolism, lead to PCH9
- AMPD2 mutations lead to GTP depletion and impaired protein synthesis
- AMPD2 is necessary for neural cell survival upon adenosine induced stress
- Cell death is prevented by bypassing the block in *de novo* purine synthesis

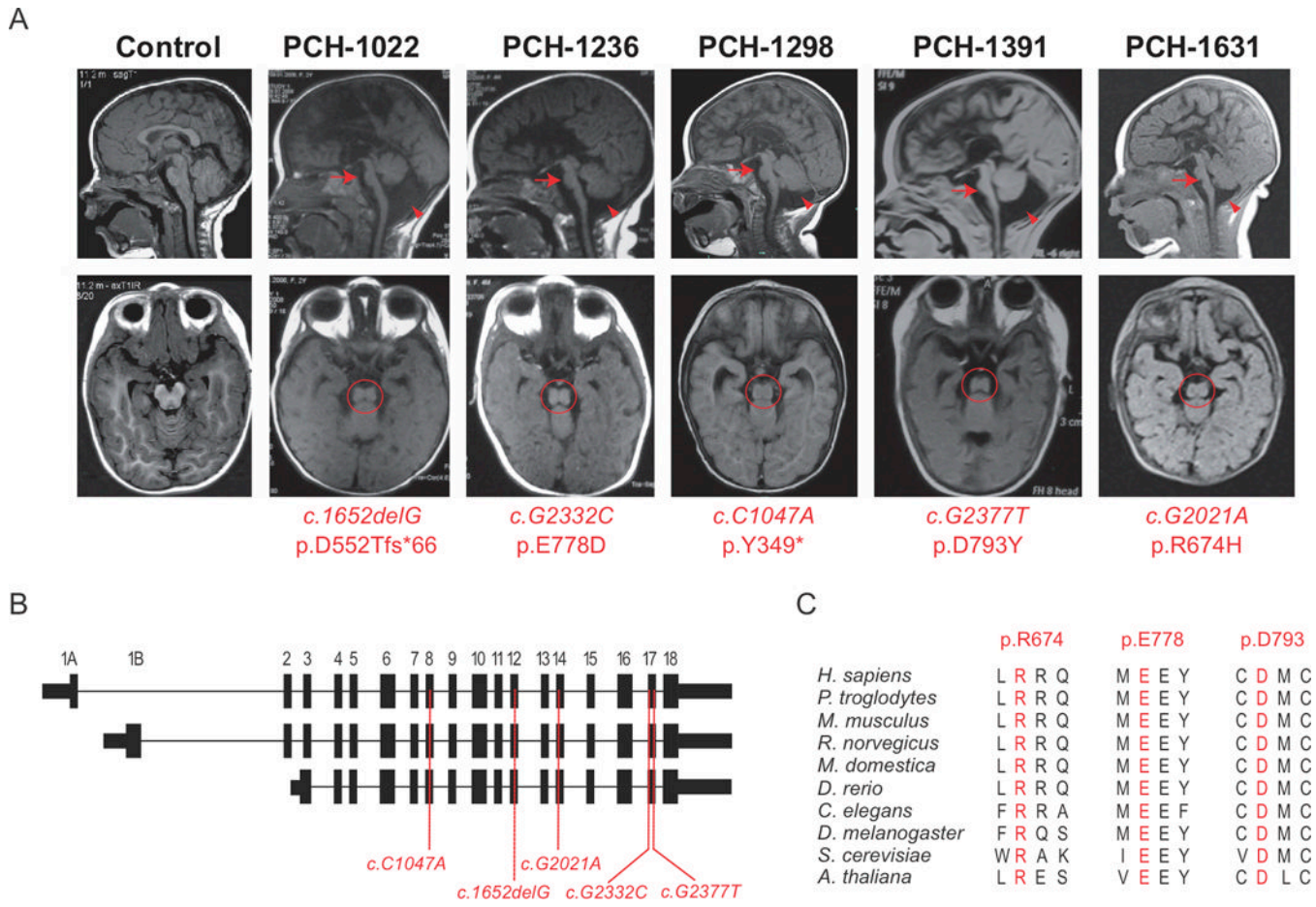

Figure 1. Recessive mutations in *AMPD2* cause loss of brainstem and cerebellar structures, typical of PCH

(A) Brain MRI from one of the affected patients for each PCH family. Control child brain MRIs are from pediatric brain atlas (http://www.seattlechildrens.org/healthcare-professionals/education/radiology/pediatricbrainatlas/). Upper: midline sagittal MRI, Lower: axial MRI at optic chiasm level. Images show smaller cerebellum (red arrowhead) and brainstem hypoplasia (red arrow) typical of PCH in all patients compared with the control. All patients show near complete absence of the corpus callosum. All patients show typical "Figure 8" shape of the brainstem (red circle). Corresponding mutation in cDNA (c) and protein (p) is below each scan. Fs: frame shift; *: stop codon.

(B) Schematic representation of three *AMPD2* isoforms. Mutations indicated relative to their position in cDNA.

(C) Mutated amino acids in PCH are fully conserved.

See also Figure S1 and Table S1.

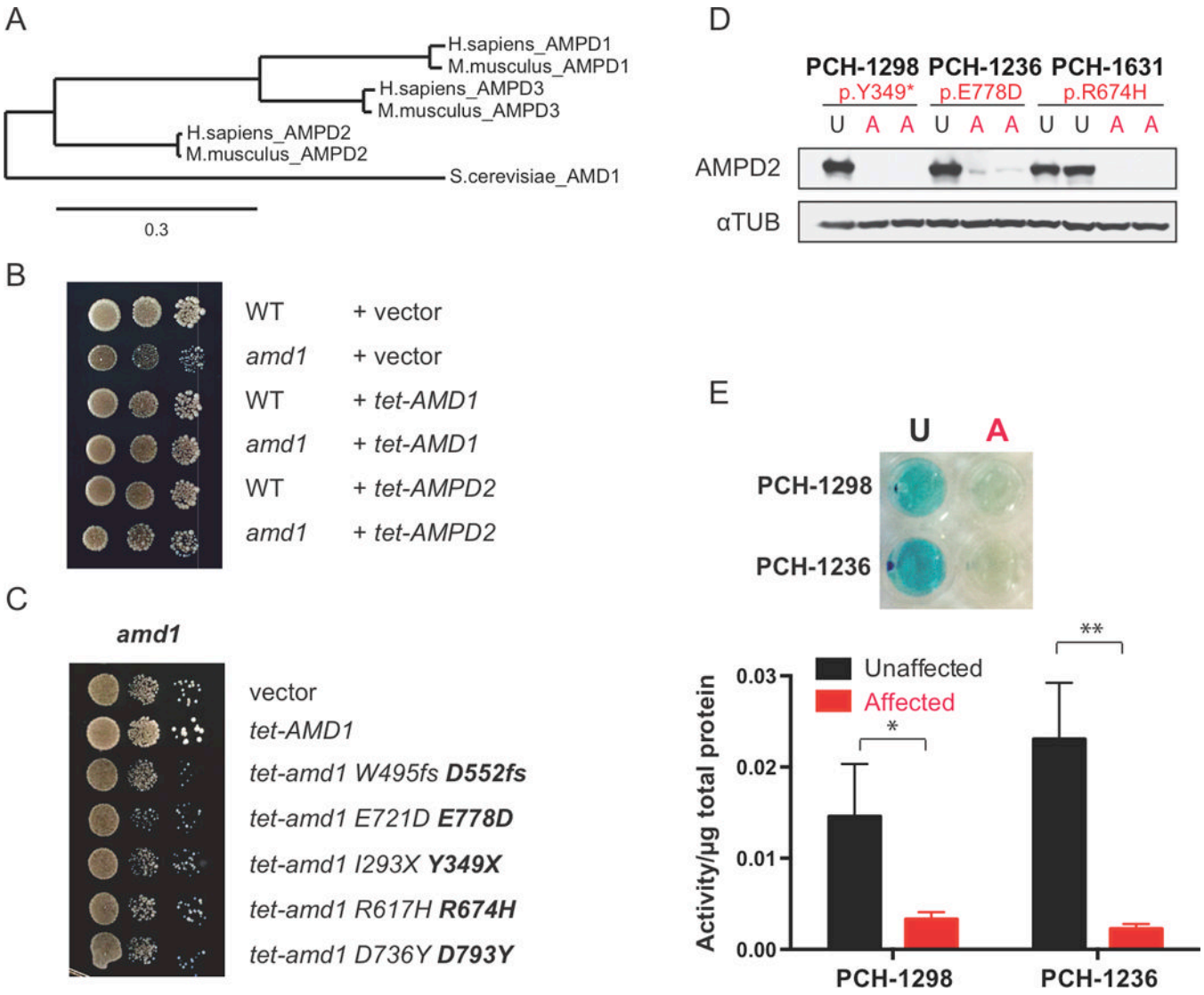

Figure 2. Mutations in *AMPD2* cause protein instability and loss of protein function

(A) Phylogenic tree representing yeast, mouse and human AMP deaminase proteins.

(B) 10-fold serial dilutions (left to right) of WT or *amd1* yeast strains transformed with yeast *AMD1* or human *AMPD2* gene on adenine-supplemented media. Yeast *amd1* mutant growth restriction is relieved by either yeast *AMD1* or human *AMPD2* forced-expression.

(C) 10-fold serial dilutions of *amd1* mutant yeast transformed with tetracycline-regulated expression of *AMD1* WT or corresponding human mutations on adenine-supplemented media in presence of 0.1µg/ml of doxycycline. Forced expression of WT but not patient mutations rescues growth restriction.

(D) Immunoblot analysis of AMPD2 levels in affected (A) and unaffected (U) fibroblasts. GAPDH is shown as loading control. Affecteds show absent or near-absent AMPD2. Corresponding *AMPD2* mutations listed below each family.

(E) Reduced AMP deaminase activity in affected (A) compared with related unaffected (U) fibroblasts, measured by standard colorimetric AMP deaminase assay. Upper: blue intensity represents relative activity. Lower: quantification of activity ±SD for three independent experiments. *P<0.05: **P<0.005. Student's t-test.

See also Figure S2.

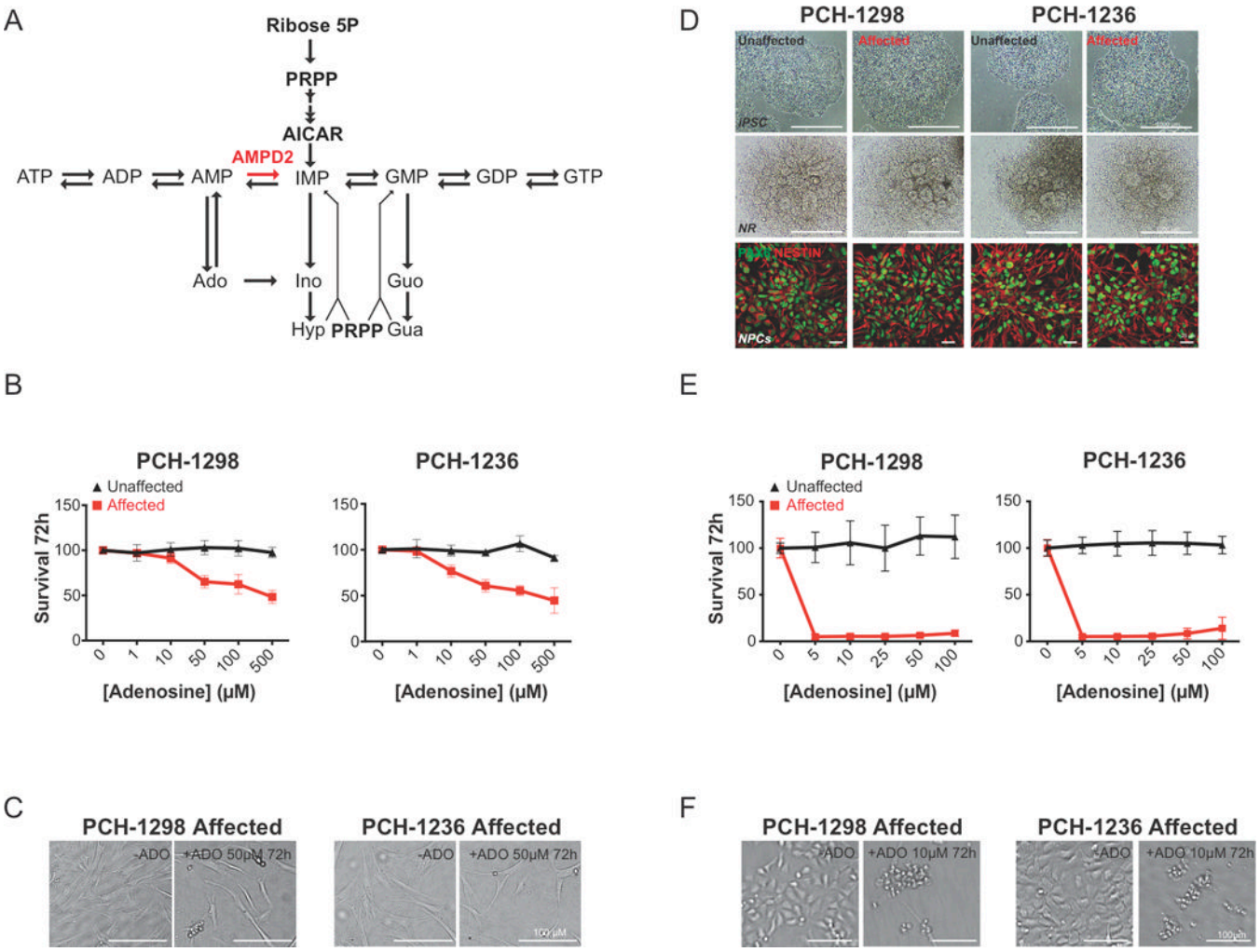

Figure 3. Adenosine supplementation reduces viability of AMPD2 deficient patient-derived cells

(A) Schematic of nucleotide metabolic pathway. Red arrow: enzymatic reaction catalyzed by AMPD2, mutated in PCH patients (red). Ado, adenosine; Gua, guanine; Guo, guanosine: Ino, inosine: Hyp, hypoxanthine: PRPP, Phosphoribosyl pyrophosphate

(B) Survival of unaffected and affected fibroblasts from families PCH-1298 and PCH-1236, cultured with escalating adenosine concentrations for 72h. Mean ±SD (four independent replicates).

(C) Bright field images for affected PCH-1298 and PCH-1236 fibroblasts in standard medium or 50μM adenosine supplemented medium, documenting modest drop in survival.

(D) Bright field images for PCH-1298 and PCH-1236 unaffected and affected derived induced pluripotent stem cells (iPSC) and neural rosettes (NR). PAX6 (green) and NESTIN (red) immunostaining in neural progenitor cells (NPCs), corresponding to one unaffected and one affected clone per family.

(E) Survival rates of unaffected and affected NPCs from families PCH-1298 and PCH-1236, cultured with escalating adenosine concentrations for 72h, showing 10-fold increase sensitivity to adenosine concentrations of NPCs compared with fibroblasts. Mean ±SD (three clones assayed at least in quadruplicates).

(F) Bright field images for affected PCH-1298 and PCH-1236 NPCs in standard medium or 10μM adenosine supplemented medium, documenting severely reduced survival.

See also Figure S3 and Table S2.

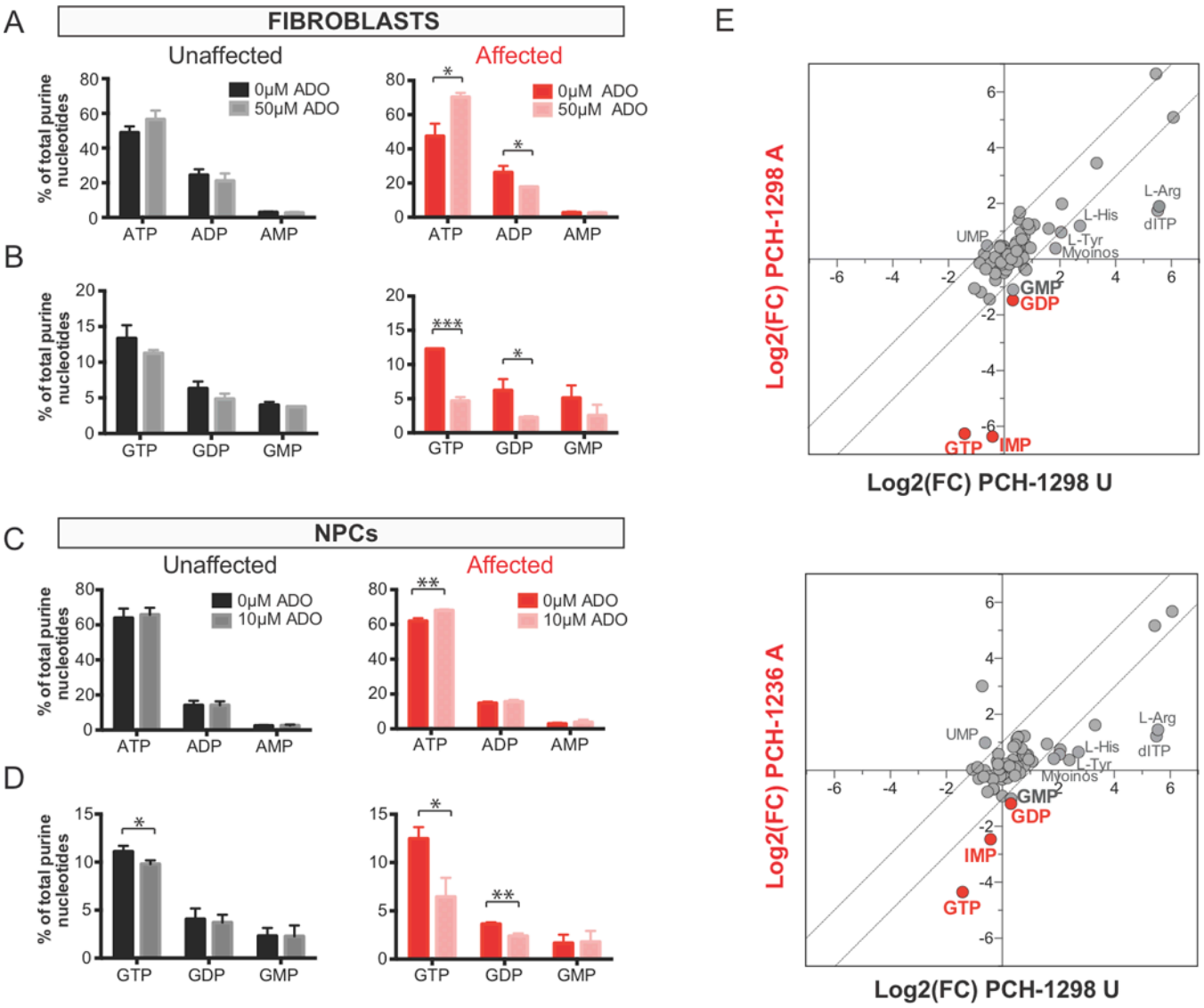

Figure 4. Adenosine supplementation induces adenosine nucleotide accumulation and severe guanine nucleotide depletion in *AMPD2*-mutant patient cells

(A–D) Percentage of adenosine (A, C) or guanine (B, D) nucleotide levels measured by HPLC in affected and unaffected fibroblasts or NPCs cultured with or without adenosine for 5h. Gray: Unaffected, Red: Affected. Mean ±SD (0μM ADO n=4; 50μM ADO n=2). *P<0.05, **P<0.0005; student's t-test.

(E) Graphical representation of LC-MS/MS data. Concentrations were used to calculate the fold change (FC) of each metabolite in 10μM vs. 0μM adenosine treatment, represented in log scale. Average $\log_2$(FC) for two affected clones in family PCH-1298 (top) and family PCH-1236 (bottom) (y-axis) and two unaffected clones (x-axis) from family PCH-1298. Dashed lines: arbitrarily defined correlation threshold. Red dots: metabolites outside the threshold limits that significantly change in affecteds and are more reduced than in unaffected (U). Guanine nucleotides and IMP are consistently reduced (red) in affected (A) NPCs.

See also Figure S4, Table S3 and S4

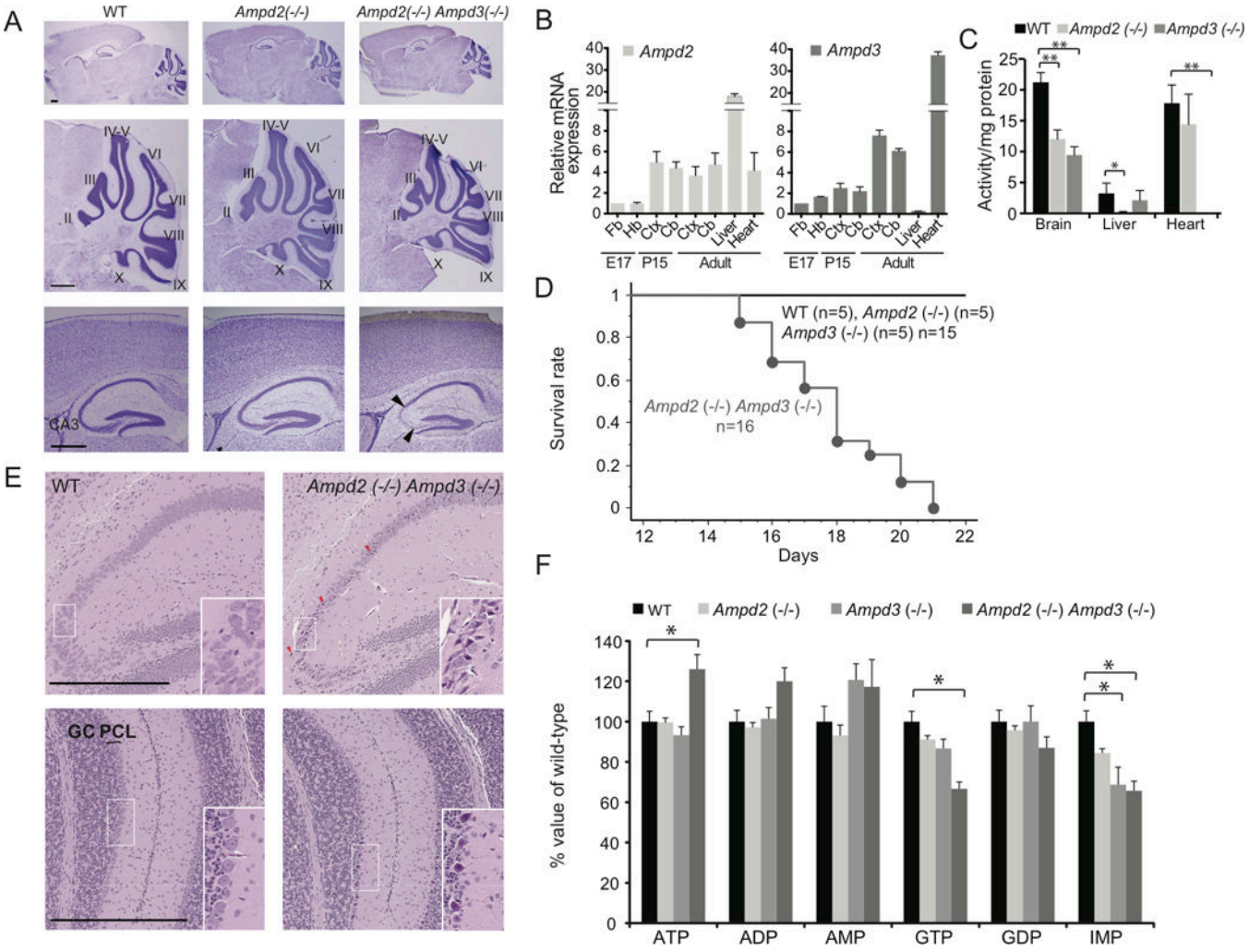

Figure 5. AMP deaminase deficiency is associated with postnatal neurodegeneration and altered nucleotide levels in mouse

(A) Parasagittal cresyl-violet sections from WT, *Ampd2* KO and *Ampd2/3* DKO at P20. Smaller size of the *Ampd2/3* DKO whole brain (upper panels) and cerebellum (middle panels) is evident. Cerebellar lobules labeled with roman numerals. Cell loss visible in the CA3 region of the hippocampus in the *Ampd2/3* DKO (lower panels, arrowheads). Scale bar, 0.5mm.

(B) qPCR of *Ampd2* and *Ampd3* normalized with *Actin* as loading control. Fb: forebrain; Hb: hindbrain; Cb: cerebellum; Ctx: cortex. E: embryonic day; P: postnatal day. Mean ±SD of three replicates.

(C) AMP deaminase activity from WT, *Ampd2* KO and *Ampd3* KO in brain, liver and heart. *Ampd2* KO and *Ampd3* KO conserve about half of WT AMP deaminase activity in brain. Mean ±SD of four replicates. *P<0.05, **P<0.0005; student's t-test.

(D) Kaplan-Meier survival curve of *Ampd2/3* DKO compared to *Ampd2* KO, *Ampd3* KO and WT. Mean of *Ampd2/3* DKO survival is 17.8±0.5 days.

(E) Parasagittal H&E sections from WT and A*mpd2/3* DKO at P15. Scattered eosinophilic neurons are visible in the hippocampus (upper panels, arrowheads) and in the Purkinje cell layer of the cerebellum (lower panels) of DKOs. Insets: Higher-magnification of pyknotic cells (dark staining). GC: cerebellar granule cell; PCL: Purkinje cell layer. Scale bar, 0.5mm.

(F) Whole brain nucleotide levels in P14 brains from the four genotypes. ATP levels were significantly increased (26%) and GTP significantly decreased (33%) in *Ampd2/3* DKO. See also Movie S1

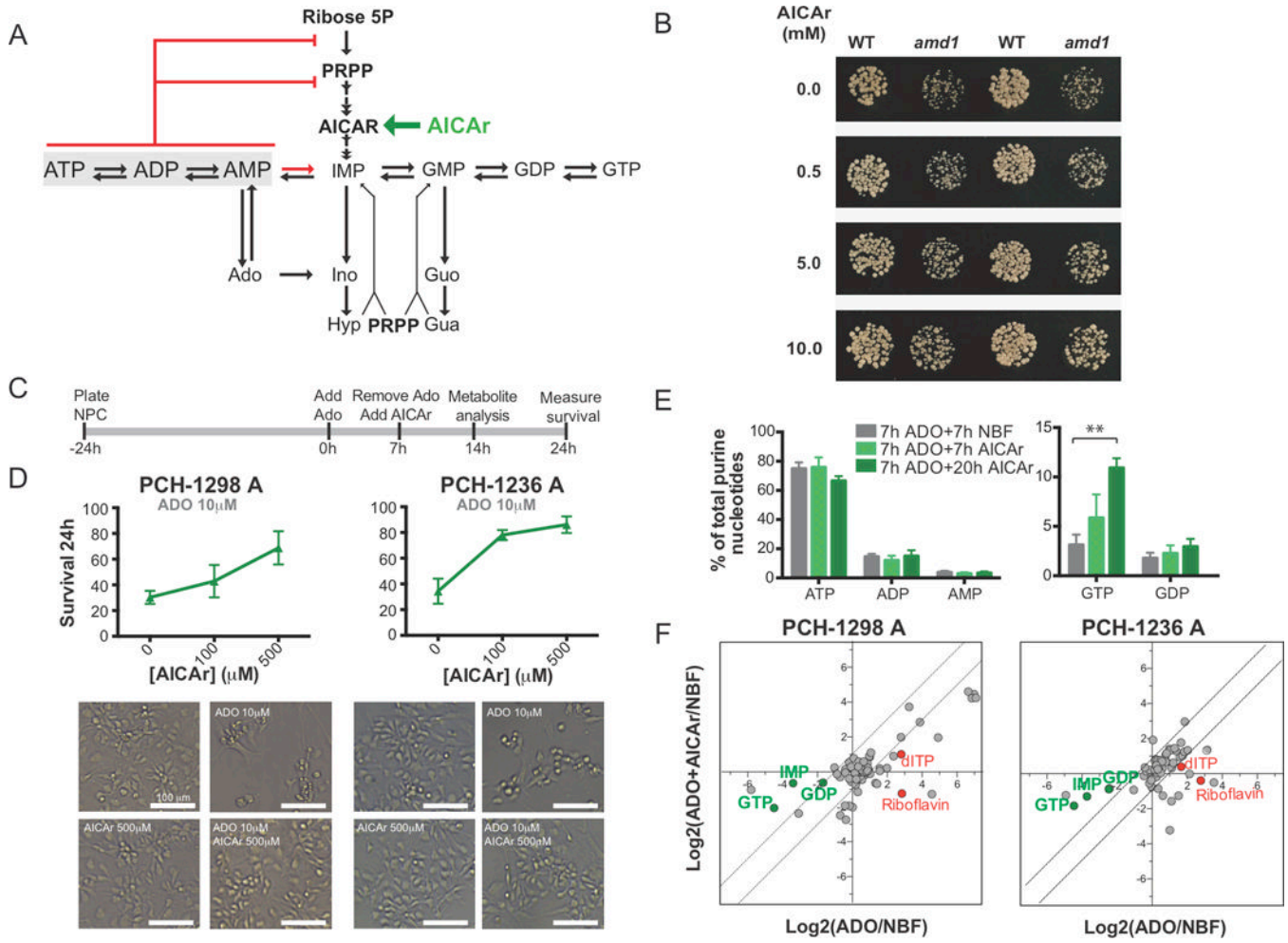

Figure 6. AICAr treatment restores cell growth in yeast and viability in patient NPCs

(A) Schematic of purine nucleotide metabolic pathway highlighting the inhibitory effect of adenosine nucleotides on *de novo* synthesis pathway (red) and the metabolic route for AICAr (green) in *AMPD2* deficient cells.

(B) Culture of identical concentration of WT and *amd1* yeast cells in presence of adenine, demonstrating rescue of growth defects upon increasing AICAr concentration.

(C) Schematic of AICAr rescue experimental protocol in human NPCs. Adenosine was added at time 0h then washed out at 7h and replaced with AICAr. Metabolites and survival were analyzed at 14h and 24h respectively.

(D) Improved survival of affected NPCs treated with increasing AICAr concentrations. Graph represents mean ±SD from two clones assayed at least in quadruplicates. Lower panels: bright field images of cells demonstrating increase in cell survival upon AICAr treatment.

(E) Percentage of adenosine (A) or guanine (B) nucleotide levels measured by HPLC in affected NPCs, cultured in adenosine for 7h followed by standard medium (NBF) or AICAr 500 μM. Data is compared to 7h adenosine + 7h standard medium to minimize the contamination from non-viable NPCs in longer cultures. GMP was non-detectable under all conditions and is thus not shown. Mean ±SD for three clones derived from PCH-1298 and PCH-1236 family affected NPCs. **P<0.005 student's t-test.

(F) Graphical representation of LC-MS/MS data. Concentrations were used to calculate the fold change (FC) of each metabolite in 10μM adenosine+standard medium (NBF) (x-axis) or

10μM adenosine+500μM AICAr (y-axis) vs. NBF. Average $\log_2$(FC) for two affected (A) clones from each family PCH-1298 (left) and family PCH-1236 (right). Dashed lines: arbitrarily defined correlation threshold. Green and red dots: metabolites outside the threshold limits that significantly increase (green) or decrease (red) with AICAr. Guanine nucleotides and IMP are significantly higher in affected NPCs that receive AICAr for 7h after adenosine challenge. Metabolites outside the graph scale are not represented (i.e. AICAr).

See also Figure S5 and Table S5.

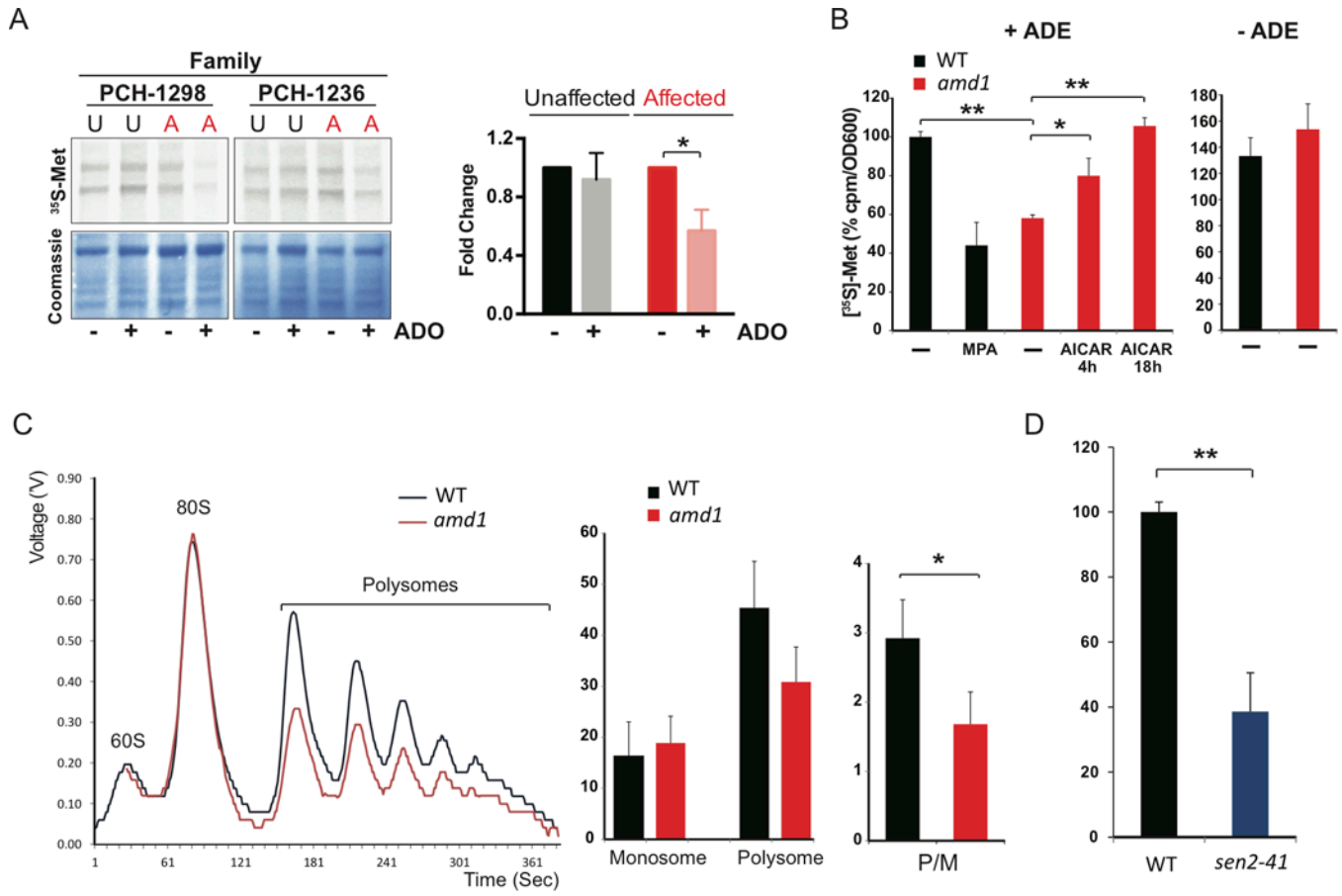

Figure 7. AMPD2 deficiency results in translation initiation blocking

(A) Metabolic labeling with [^{35}S]-Methionine of NPCs shows reduced incorporation in affecteds (A) compared with unaffecteds (U) in presence of adenosine (+: 10μM for 5h). Upper panel: [^{35}S] autoradiogram. Lower panel: Coomassie staining. Graph: autoradiogram quantification normalized for total protein for three NPC clones.

(B) Metabolic labeling with [^{35}S]-Methionine of yeast cells grown in SD-CASA media supplemented with adenine. Mycophenolyc acid (MPA 30μg/ml, inhibits guanine nucleotide synthesis) used as positive control. A decrease of 41% in the rate of incorporation of [^{35}S]-Methionine in *amd1* strain is rescued by AICAr incubation prior to metabolic labeling in a time-dependent fashion, whereas no difference was detected in the absence of adenine (right)

(C) Representative polysome profiles of WT and *amd1* mutant strains grown with adenine. Polysome (P) and monosome (M; 80S peak) profiles were quantified from three independent experiments. Polysome to monosome ratio (P/M) suggests a defect in protein translation initiation (right).

(D) Metabolic labeling with [^{35}S]-Methionine of WT and *sen2-41* mutant at non permissive temperature.

*P<0.05; **P<0.0005, student's t-test, all graphs show mean ±SD